

# Modeling Quantum Autoencoder Trainable Kernel for IoT Anomaly Detection

Swathi Chandrasekhar, Shiva Raj Pokhrel, Swati Kumari and Navneet Singh

**Abstract**—Escalating cyber threats and the high-dimensional complexity of IoT traffic have outpaced classical anomaly detection methods. While deep learning offers improvements, computational bottlenecks limit real-time deployment at scale. We present a quantum autoencoder (QAE) framework that compresses network traffic into discriminative latent representations and employs quantum support vector classification (QSVC) for intrusion detection. Evaluated on three datasets, our approach achieves improved accuracy on ideal simulators and on the IBM Quantum hardware (ibm\_fez)—demonstrating practical quantum advantage on current NISQ devices. Crucially, moderate depolarizing noise acts as implicit regularization, stabilizing training and enhancing generalization. This work establishes quantum machine learning as a viable, hardware-ready solution for real-world cybersecurity challenges.

**Index Terms**—Quantum Autoencoders, Quantum machine learning, Quantum support vector classifiers

## I. INTRODUCTION

Securing Internet of Things (IoT) networks demands anomaly detectors [1], [2], [3] that can model high-dimensional, nonstationary traffic with limited compute budgets. Classical deep models help, but their footprint and training instability under distribution drift are problematic at the network edge.

The development of deep learning techniques brought unprecedented capabilities to anomaly detection [2]. Neural networks, particularly autoencoders and recurrent neural networks (RNNs), demonstrated the ability to learn complex patterns in high-dimensional data without extensive feature engineering. Autoencoders, for instance, were used to compress network traffic data [4] into lower-dimensional representations and identify anomalies based on reconstruction errors [5]. These methods were further enhanced by distributed computing frameworks, which enabled the analysis of massive datasets. However, even with these improvements, deep learning models remain constrained by the computational limits of classical hardware, especially in real-time applications for large-scale networks.

Authors are from the Quantum Research Group at School of IT, Deakin University, Geelong, Australia; email: shiva.pokhrel@deakin.edu.au.

Quantum computing [6] has emerged as a promising solution to these challenges. By leveraging the principles of superposition, entanglement, and interference, quantum computers can process high-dimensional data and solve optimization problems exponentially faster than classical systems [6], [7]. Quantum algorithms offer significant speedups for tasks like dimensionality reduction and clustering. In the context of network intrusion detection, quantum machine learning models, including quantum support vector machines (QSVMs) and quantum autoencoders (QAE), have the potential to detect complex and subtle anomalies [3]. In Fig. 1, we present a high level view of or idea of the end-to-end quantum autoencoder framework for anomaly detection that standardizes and encodes data, jointly learns compression and a quantum kernel, and then classifies anomalies using a QSVC in the optimized quantum feature space.

In this paper, we propose a quantum-enhanced anomaly detection framework that integrates coherence-driven feature compression, task-adaptive kernel learning, and noise-aware optimization. A SWAP-test-based QAE compresses high-dimensional traffic data into compact latent states while preserving discriminative structure, and a trainable quantum kernel—optimized jointly with the QAE via SPSA—aligns the latent space to the downstream classification task. We show that moderate depolarizing noise acts as an implicit regularizer that stabilizes gradients and improves generalization. The resulting QAE–QSVC model achieves over 92% accuracy on Bot\_IoT, IoT23, and KDD99 in noiseless simulations, and maintains  $\geq 83\%$  accuracy on IBM Quantum hardware, demonstrating practical feasibility. The design remains resource-efficient through amplitude encoding with  $n_q = \lceil \log_2 d \rceil$  qubits and shallow circuits, enabling deployment in constrained IoT settings. Our pipeline (Fig. 1) performs classical preprocessing, amplitude encoding, QAE-based latent learning, task-adapted kernel optimization, and QSVC training, evaluated under both ideal and noisy quantum regimes.

### A. Data Encoding and Preprocessing

The preprocessed dataset samples were subjected to a three-stage pipeline to ensure compatibility with quan-

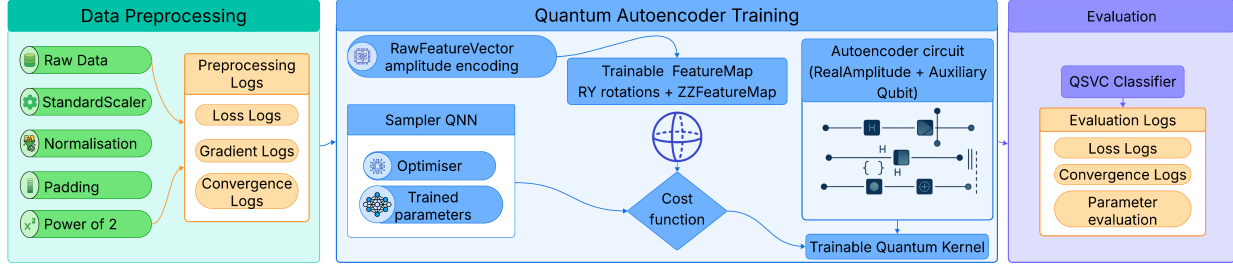


Fig. 1: Overall pipeline of the proposed quantum autoencoder-based anomaly detection framework. (i) data preprocessing, including standardization, normalization, and power-of-two padding (ii) quantum autoencoder training, where RawFeatureVector amplitude encoding, a trainable feature map, and the autoencoder circuit are optimized via a sampler QNN and cost function to learn compressed latent representations and a trainable quantum kernel; and (iii) evaluation, in which a QSVC classifier uses the learned quantum kernel to perform anomaly detection.

tum state representation. Each sample  $\mathbf{x} \in \mathbb{R}^d$  underwent standardization via z-score normalization:  $\mathbf{x}_{\text{scaled}} = \frac{\mathbf{x} - \mu}{\sigma}$ , where  $\mu$  and  $\sigma$  represent the feature-wise mean and standard deviation computed across the training corpus. Subsequently, L2 normalization was applied to satisfy the unit norm constraint required for quantum amplitude encoding:  $\mathbf{x}_{\text{norm}} = \frac{\mathbf{x}_{\text{scaled}}}{\|\mathbf{x}_{\text{scaled}}\|_2}$ .

To map the  $d$ -dimensional feature space onto a quantum register, we computed the minimum qubit requirement as  $n_q = \lceil \log_2(d) \rceil$ , yielding a  $2^{n_q}$ -dimensional Hilbert space. Zero-padding was applied to extend each sample to match this dimension:  $\mathbf{x}_{\text{padded}} = [\mathbf{x}_{\text{norm}}, \underbrace{0, \dots, 0}_{2^{n_q} - d}]^T$ .

**Amplitude Encoding Implementation:** The RawFeatureVector [8] circuit directly encodes the classical feature vector into quantum amplitudes via state preparation:  $|\psi(\mathbf{x})\rangle = \sum_{i=0}^{2^{n_q}-1} x_i |i\rangle$  where  $x_i$  represents the  $i$ -th component of  $\mathbf{x}_{\text{padded}}$ . This encoding scheme, implemented through the feature map  $\text{fm} = \text{RawFeatureVector}(2 * \text{num\_qubits})$ , maps classical data into the computational basis states of an  $n_q$ -qubit system, preserving the L2 norm as the total probability:  $\sum |x_i|^2 = 1$ .

### B. Modeling Trainable Quantum Autoencoder Kernel

The QAE was designed to compress the  $n_q$ -qubit encoded state into an  $n_l$ -qubit latent representation, discarding  $n_t$  qubits of redundant information, where  $n_t = n_q - n_l$ . The architecture employs a  $(n_l + 2n_t + 1)$ -qubit system partitioned into a latent register of  $n_l$  qubits preserving compressed information, trash register A of  $n_t$  qubits containing discarded information, trash register B of  $n_t$  reference qubits initialized to  $|0\rangle$ , and an auxiliary qubit for fidelity measurement [9].

**1) Encoder Circuit:** The variational encoder circuit  $U_{\text{enc}}(\theta)$  was constructed using the RealAmplitudes ansatz with  $n$  repetitions, applied to the first  $(n_l + n_t)$  qubits:  $U_{\text{enc}}(\theta) = \prod_{r=1}^n [U_{\text{ent}} \cdot U_{\text{rot}}(\theta_r)]$  where  $U_{\text{rot}}$  consists of parameterized RY rotations:  $U_{\text{rot}}(\theta_r) = \bigotimes_{j=0}^{n_l+n_t-1} RY(\theta_{r,j})$  and  $U_{\text{ent}}$  implements a linear entanglement pattern using CX gates connecting adjacent qubits. The total parameter count for the encoder is  $n \times (n_l + n_t)$  parameters.

**2) SWAP Test for Fidelity Measurement:** The compression quality was evaluated using a quantum SWAP test circuit that measures the fidelity between trash registers A and B. The auxiliary qubit was prepared in superposition, followed by controlled-SWAP operations. After applying the inverse Hadamard  $H^\dagger$ , the measurement outcome probability on the auxiliary qubit. The reconstruction loss  $L_{\text{AE}}$  is defined as the expectation of measuring  $|1\rangle$ , which quantifies the information retained in the trash qubits. Optimal compression is achieved when trash A and trash B are maximally entangled with the latent space, yielding  $P(|1\rangle) \rightarrow 0$ .

**3) Training Protocol:** The autoencoder was trained using the COBYLA optimizer, a gradient-free derivative of Powell's method that constructs successive linear approximations of the objective function. The loss function was estimated via mini-batch sampling, where multiple batches were randomly drawn from the training pool at each iteration. The stochastic batching strategy provides variance estimates for loss uncertainty quantification:  $\sigma_{\text{loss}} = \sqrt{\frac{1}{B-1} \sum_{b=1}^B (\hat{L}_b - \hat{L}_{\text{AE}})^2}$  where  $B$  denotes the number of batches per iteration and  $\hat{L}_b$  represents the loss computed on batch  $b$ . This variance was logged alongside 95% confidence intervals:  $[\mu - 1.96\sigma, \mu + 1.96\sigma]$ .

**4) Latent Feature Extraction:** Post-training, the encoder circuit (excluding the SWAP test) was used

to extract compressed representations. For each input  $\mathbf{x}_{\text{padded}}$ , the quantum state after encoding is:  $|\phi(\mathbf{x}, \theta^*)\rangle = U_{\text{enc}}(\theta^*)|\psi(\mathbf{x})\rangle$  where  $\theta^*$  denotes the optimized parameters. The latent features were extracted by computing the probability distribution over the  $n_l$ -qubit latent subspace.

### C. Trainable Quantum Kernel

The kernel matrix element between samples  $\mathbf{z}_i$  and  $\mathbf{z}_j$  is computed via the ComputeUncompute fidelity protocol:

$$K(\mathbf{z}_i, \mathbf{z}_j; \phi) = |\langle 0^{\otimes n_k} | \Phi^\dagger(\mathbf{z}_j, \phi) \Phi(\mathbf{z}_i, \phi) | 0^{\otimes n_k} \rangle|^2 \quad (1)$$

This is estimated via sampling with a fixed number of shots per circuit execution  $\hat{K}(\mathbf{z}_i, \mathbf{z}_j; \phi) = \frac{N_{|0^{\otimes n_k}\rangle}}{N_{\text{shots}}}$  where  $N_{|0^{\otimes n_k}\rangle}$  is the count of all-zero measurement outcomes.

The kernel parameters  $\phi$  were optimized using the QSVC loss function, which maximizes the margin in the quantum feature space [10]. For a binary classification task with labels  $y \in \{-1, +1\}$ , the loss is  $L_{\text{QSVC}}(\phi) = \frac{1}{2} \boldsymbol{\alpha}^T \mathbf{K}(\phi) \boldsymbol{\alpha} - \sum_{i=1}^N \alpha_i$

The kernel parameters were optimized using the SPSA algorithm. SPSA is a gradient-free stochastic optimization method particularly suited for noisy objective functions, as it estimates the gradient using only two function evaluations per iteration regardless of the parameter dimension. The hyperparameters include maximum iterations, learning rate  $\alpha_k$ , and perturbation magnitude  $c_k$ . The gradient estimate at iteration  $k$  is computed via symmetric finite differences:  $\hat{\nabla} L(\phi_k) = \frac{L(\phi_k + c_k \Delta_k) - L(\phi_k - c_k \Delta_k)}{2c_k} \Delta_k$  where  $\Delta_k$  is a random perturbation vector with elements sampled from  $\{-1, +1\}$ .

### D. Quantum Support Vector Classification

The optimized quantum kernel  $K(\mathbf{z}_i, \mathbf{z}_j; \phi^*)$  was used to train a QSVC by solving the optimization problem:

$$\max_{\boldsymbol{\alpha}} \sum_{i=1}^N \alpha_i - \frac{1}{2} \sum_{i=1}^N \sum_{j=1}^N \alpha_i \alpha_j y_i y_j K(\mathbf{z}_i, \mathbf{z}_j; \phi^*) \quad (2)$$

subject to  $\sum_{i=1}^N \alpha_i y_i = 0$  and  $0 \leq \alpha_i \leq C$ , where  $C$  is the regularization parameter that controls the trade-off between the maximization of the margin and the minimization of the training error. The QSVC exploits the capacity of the quantum kernel to implicitly embed data in an exponentially large feature space, where the kernel function  $K(\mathbf{z}_i, \mathbf{z}_j; \phi^*)$  corresponds to the inner product of quantum states. The entanglement structure encoded in the feature map captures complex non-linear relationships that are difficult to model classically, while the support vectors and their dual coefficients  $\alpha_i$  define the decision boundary in this high-dimensional quantum space.

## II. RESULTS

Dataset	Avg <i>loss_std</i>	Avg <i>lower_bound</i>	Avg <i>upper_bound</i>
Bot_IoT	0.0191	0.1843	0.2590
IoT23	0.0171	0.2576	0.3244
KDD	0.0213	0.2826	0.3660
Depolarizing Noise			
Bot_IoT	0.0168	0.2906	0.3564
IoT23	0.0302	0.1513	0.2699
KDD	0.0169	0.2644	0.3308

TABLE I: Average training loss variability and confidence bounds across datasets Bot\_IoT, IoT23, and KDD for the quantum autoencoder under both noiseless and depolarizing noise conditions.

## III. PERFORMANCE EVALUATION

This section presents the experimental results obtained using the proposed QAE-QSVC for anomaly detection across multiple network intrusion datasets, Bot\_IoT, IoT23, and KDD99. Both ideal and noisy quantum scenarios were evaluated using Aer simulation backends and real IBM Quantum hardware (ibm\_fez).

*Training Loss Analysis.* Figure 2 illustrates the convergence patterns for each dataset under noisy and noise-free conditions. As observed, the QAE demonstrated stable convergence, with loss values consistently decreasing across iterations. In the Bot\_IoT dataset, noise-free training yielded a lower loss floor ( $\approx 0.20$ ) compared to the noisy configuration ( $\approx 0.30$ ), indicating the sensitivity of the circuit to accumulated decoherence. Conversely, in IoT23 and KDD datasets, the inclusion of noise led to enhanced regularization, stabilizing training oscillations after initial iterations. Table I summarizes the average standard deviation and bound metrics for each case, where the lower standard deviation across noise conditions reflects the robustness of our hybrid optimization loop.

*Gradient Behavior and Stability.* Gradient norm analysis across all datasets Figure 3 reveals distinct quantum noise propagation patterns. Bot\_IoT and KDD99 exhibited higher gradient magnitudes in the presence of noise, while IoT23 maintained comparatively smoother gradient transitions, demonstrating greater resilience of its latent representation. Normalized gradients emphasize reduced quantum circuit instability due to controlled learning rate and encoder compression.

*Coefficient of Variation Analysis.* Figures 4 present the coefficient of variation computed for autoencoder reconstruction and kernel evaluations. Lower variation trends in most noisy cases demonstrate that depolarizing noise introduces slight regularization rather than destructive interference, stabilizing the feature space embedding, particularly evident in KDD99.

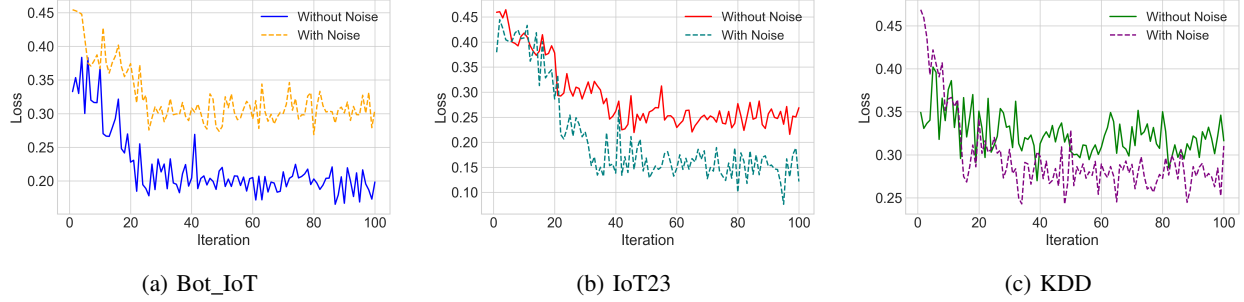


Fig. 2: Training loss curves for the quantum autoencoder on Bot\_IoT, IoT23, and KDD datasets under noiseless and depolarizing noise conditions showing convergence of model across iterations.

Dataset	Train Acc	Test Acc	Train Prec	Test Prec	Train Rec	Test Rec	Train F1	Test F1	Time (s)
Bot_IoT	0.9962	0.9242	0.9960	0.9247	0.9962	0.9242	0.9961	0.9294	157369.7
IoT23	0.9875	0.9950	0.9562	0.9650	0.9875	0.9500	0.9453	0.9268	99167.8
KDD99	0.9875	0.9766	0.9874	0.9543	0.9875	0.9857	0.9874	0.9766	84069.4
Depolarizing Noise									
Bot_IoT	0.9734	0.9545	0.9748	0.9581	0.9738	0.9545	0.9734	0.9543	91706.6
IoT23	0.9833	0.9737	0.9973	0.9836	0.9833	0.9833	0.9283	0.9222	86906.5
KDD99	0.9875	0.9833	0.9884	0.9847	0.9874	0.9833	0.9876	0.9836	86245.4

TABLE II: Performance on of the QAE–QSVC architecture on the Aer simulator under noiseless and depolarizing noise settings.

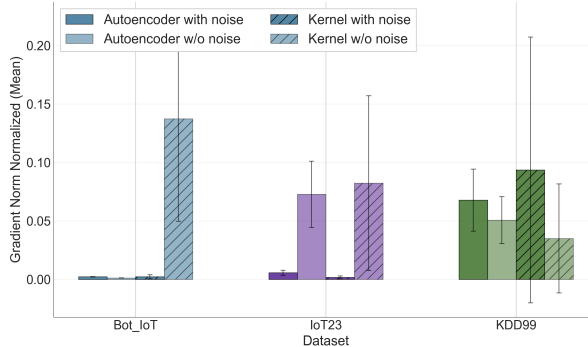


Fig. 3: Normalized gradient for autoencoder and kernel training phases under depolarizing noise as well for Bot\_IoT, IoT23, and KDD

*Performance on Simulator and Real Hardware.* Table II summarizes the performance achieved using the Aer simulator. Across all datasets, the QAE+QSVC achieved test accuracies above 92%, confirming strong generalization after quantum state compression. Even with depolarizing noise enabled, the model retained accuracy above 95% for most datasets.

Execution on the IBM Quantum system (*ibm\_fez*), which consists of the qubit topology shown in Figure 5, validated the feasibility of performing quantum autoencoder operations on real hardware despite calibration and readout errors. Due to runtime constraints (10 minutes) and limited qubit allocation, the tests were executed with reduced samples on two datasets. Even under such

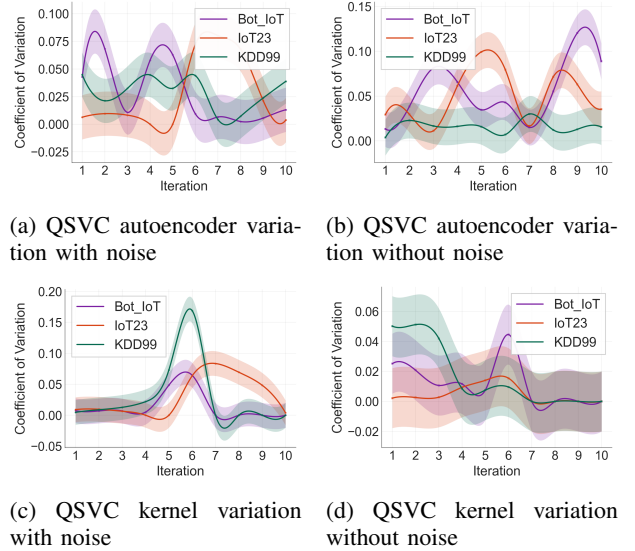


Fig. 4: Coefficient of variation of loss estimates for the QSVC autoencoder and kernel phases, comparing noisy and noiseless configurations.(a) and (b) show the variability during the autoencoder phase, while (c) and (d) depict the kernel phase across training iterations.

limitations, accuracies above 83% were achieved, as shown in Table III. These results strongly suggest that, with extended runtime and noise mitigation resources, the proposed QAE-QSVC approach could scale toward near-ideal accuracy.

Dataset	Accuracy	Precision	Recall	F1-score	Time
Bot_IoT	0.8333	0.8809	0.8333	0.8333	353
IoT23	0.8437	0.7500	0.7500	0.7447	212

TABLE III: Qubit coupling map of the IBM Quantum *ibm\_fez* device used for hardware experiments.

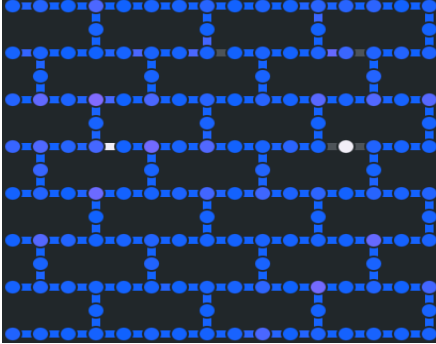


Fig. 5: Performance of the QAE–QSVC model on IBM Quantum hardware (*ibm\_fez*) for Bot\_IoT and IoT23, demonstrating the practical feasibility of deploying quantum autoencoder-based anomaly detection on current NISQ devices.

Overall, these results confirm that the proposed hybrid quantum framework not only achieves high classification performance under simulation but also sustains practical accuracy on real quantum devices. The consistent gradient stability, bounded loss, and low coefficient of variation reinforce the reliability and scalability of QAE based network anomaly detection.

To contextualize our results, we directly compare with the QAE-based anomaly detection framework of [3] (Framework 1: QAE + one-class SVM) on overlapping datasets. On *KDD99*, their reported 97.48% accuracy and 97.19% F1 are surpassed by our noisy QAE–QSVC, which attains 98.33% accuracy and 98.36% F1. The gap is even larger on *IoT23*: their 82.53% accuracy and 79.69% F1 contrast with our 97.37% accuracy and 92.22% F1 under depolarizing noise, corresponding to absolute gains of approximately 15 and 13 percentage points, respectively (Table IV). The underlying difference is that [11] applies PCA before the QAE, discarding potentially discriminative variance. In sharp contrast, our approach performs no classical dimensionality reduction; all compression occurs within the coherence-driven QAE and is paired with supervised margin-based classification, yielding consistently superior detection performance.

#### IV. CONCLUSION

This work shows that quantum autoencoding is a strong backbone for anomaly detection in large-scale

TABLE IV: Comparative evaluation of the proposed QAE–QSVC framework with [3] Framework 1 on ideal and DP:depolarising noise

Dataset	Method	Test Acc	Test F1
KDD99	QAE + OC-SVM [3]	97.48	97.19
This work	QAE–QSVC (ideal)	97.66	97.66
This work	QAE–QSVC (DP)	<b>98.33</b>	<b>98.36</b>
IoT23	QAE + OC-SVM [3]	82.53	79.69
This work	QAE–QSVC (ideal)	<b>99.50</b>	<b>92.68</b>
This work	QAE–QSVC (DP)	97.37	92.22

IoT networks. By combining a coherence-driven Quantum Autoencoder (QAE) with a Quantum Support Vector Classifier (QSVC), we build a hybrid model that learns compact, discriminative latent representations directly from amplitude-encoded traffic data. The approach achieves high detection accuracy across multiple intrusion datasets while requiring far fewer computational resources than classical deep learning methods. A SWAP-test-based fidelity objective preserves task-relevant structure, and a trainable quantum kernel improves separability in the latent space. Experiments under ideal and noisy conditions demonstrate robustness, with quantum noise acting as a useful regularizer that enhances generalization. Tests on real IBM Quantum hardware further confirm the framework’s practicality.

#### REFERENCES

- [1] Y. N. Soe, Y. Feng, P. I. Santosa, R. Hartanto, and K. Sakurai, “Rule generation for signature based detection systems of cyber attacks in iot environments,” *Bulletin of Networking, Computing, Systems, and Software*, vol. 8, no. 2, pp. 93–97, 2019.
- [2] G. Pang, C. Shen, L. Cao, and A. V. D. Hengel, “Deep learning for anomaly detection: A review,” *ACM computing surveys (CSUR)*, vol. 54, no. 2, pp. 1–38, 2021.
- [3] M. Hdaib, S. Rajasegarar, and L. Pan, “Quantum deep learning-based anomaly detection for enhanced network security,” *Quantum Machine Intelligence*, vol. 6, no. 1, p. 26, 2024.
- [4] A. Javaid, Q. Niyaz, W. Sun, and M. Alam, “A deep learning approach for network intrusion detection system,” in *Proceedings of the 9th EAI International Conference on Bio-inspired Information and Communications Technologies (formerly BIONETICS)*, pp. 21–26, ICST, 2016.
- [5] R. Gupta, D. Saxena, I. Gupta, A. Makkar, and A. Kumar Singh, “Quantum machine learning driven malicious user prediction for cloud network communications,” *IEEE Networking Letters*, vol. 4, no. 4, pp. 174–178, 2022.
- [6] H. Oh and D. K. Park, “Quantum support vector data description for anomaly detection,” *Machine Learning: Science and Technology*, vol. 5, no. 3, p. 035052, 2024.
- [7] N. Singh and S. R. Pokhrel, “Modeling feature maps for quantum machine learning,” *arXiv preprint arXiv:2501.08205*, 2025.
- [8] M. E. Sahin, E. Altamura, O. Wallis, S. P. Wood, A. Dekusar, D. A. Millar, T. Imamichi, A. Matsuo, and S. Mensa, “Qiskit machine learning: an open-source library for quantum machine learning tasks at scale on quantum hardware and classical simulators,” 2025.
- [9] Y. Mirsky, T. Doitshman, Y. Elovici, and A. Shabtai, “Kitsune: An ensemble of autoencoders for online network intrusion detection,” in *2018 Network and Distributed System Security Symposium (NDSS)*, Internet Society, 2018.

- [10] S. Chandrasekhar, S. R. Pokhrel, and N. Singh, “Adapting quantum machine learning for energy dissociation of bonds,” *ChemRxiv*, 2025.
- [11] M. Hdaib, S. Rajasegarar, and L. Pan, “Quantum autoencoder frameworks for network anomaly detection,” in *International Conference on Neural Information Processing*, pp. 69–82, Springer, 2023.